

# REVISED LENS MODEL FOR THE MULTIPLY-IMAGED LENSED SUPERNOVA, “SN Refsdal” IN MACS J1149+2223\*

KEREN SHARON<sup>1</sup>, TRACI L. JOHNSON<sup>1</sup>,  
*ApJ in prep: draft date April 18, 2022*

## ABSTRACT

We present a revised lens model of MACS J1149+2223, in which the first resolved multiply-imaged lensed supernova was discovered. The lens model is based on the model of Johnson et al. (2014) with some modifications. We include more lensing constraints from the host galaxy of the newly discovered supernova, and increase the flexibility of the model in order to better reproduce the lensing signal in the vicinity of this galaxy. The revised model accurately reconstructs the positions of the lensed supernova, provides magnifications, and predicts the time delay between the instances of the supernova. Finally, we reconstruct the source image of the host galaxy, and position the supernova on one of its spiral arms. Products of this lens model are available to the community through MAST.

*Subject headings:* galaxies: clusters: general — gravitational lensing: strong — galaxy clusters: individual: MACS J1149+2223 — supernovae: individual (“SN Refsdal”)

## 1. INTRODUCTION

A discovery of a multiply-imaged lensed supernova (SN) has always been considered a low probability, high gain possibility in SN surveys (e.g., Refsdal 1964, Kovner & Paczynski 1988), especially those focused on fields of lensing clusters. Although several lensed SN candidates have been reported (Quimby et al. 2014, Patel et al. 2014, Goobar et al. 2009), the recent discovery of a lensed SN in the field of MACS J1149+2223 (Kelly et al. 2014a, 2014b) is the first reported case of multiply-imaged one, whose instances are detected and resolved.

“SN Refsdal” was discovered in *HST* WFC3/IR data obtained as part of the Grism Lens Amplified Survey from Space (GLASS; GO 13459, PI: Treu) between 2014 November 3 and 2014 November 20. We refer the reader to Kelly et al. (2014b) for details of the discovery. The host of “SN Refsdal” is a multiply-imaged face-on spiral galaxy at  $z = 1.491$ , lensed by the cluster halo into three full images and one partial image (Smith et al. 2009), and further distorted by lensing perturbations by cluster galaxies. As we will show in the following sections, “SN Refsdal” occurred in one of the spiral arms of this galaxy, which happens to be going through secondary lensing by a cluster-member galaxy. The SN is thus lensed into four images around that cluster galaxy, in a configuration known as “Einstein Cross” (Kelly et al. 2014a).

MACS J1149+2223 is an X-ray bright, strong lensing cluster at  $z = 0.543$  (Ebeling et al. 2007). Strong lensing models of MACS J1149+2223 were published by Smith et al. (2009) and Zitrin et al. (2009) based on shallow *HST* imaging (GO-9722, PI: Ebeling) and by Zitrin et al. (2011, 2014), and Rau et al. (2014) based on data from the Cluster Lensing and Supernova Survey with Hubble

(CLASH) multicycle program (PI: Postman; Postman et al. 2012). Smith et al. (2009) also measured the spectroscopic redshifts of some of the lensed sources behind MACS J1149+2223. MACS J1149+2223 was recently selected as one of the Hubble Frontier Fields (HFF, PI: Lotz) to be deeply imaged by *HST*. Preliminary lens models were derived by several teams prior to the deep HFF imaging, using a close to uniform set of constraints, but varying in lens modeling approaches, codes, and assumptions (PI: Sharon – Johnson et al. 2014; PIs: Kneib & Natarajan, CATS – Richard et al. 2014; PI: Bradač; PIs: Zitrin & Merten; PI: Williams). The results of these models were made available to the community through Mikulski Archive for Space Telescopes (MAST<sup>3</sup>). While these models provide a good description of the lens plane, they were not tailored to fit any one lensed source in particular, but to provide the best mass distribution and magnification estimates given a large set of constraints coming from lensed galaxies at different redshifts. This approach allows a better sampling of the slope of the mass distribution and facilitates studies of the magnified background Universe.

In this letter, we revise the model of Johnson et al. (2014; hereafter J14) and present a new lens model for MACS J1149+2223, that better reproduces the lensing evidence at the vicinity of the multiply-imaged lensed SN. We assume a flat cosmology with  $\Omega_{\Lambda} = 0.7$ ,  $\Omega_m = 0.3$ , and  $H_0 = 70 \text{ km s}^{-1} \text{ Mpc}^{-1}$ . In this cosmology,  $1''$  corresponds to 6.37 kpc at the cluster redshift,  $z = 0.543$ . Magnitudes are reported in the AB system.

## 2. LENS MODEL

We base our lensing analysis on the model presented by J14, with a few modifications, as described below. The model is computed with Lenstool (Jullo et al. 2007), using Markov Chain Monte Carlo (MCMC) sampling of the parameter space.

The positional constraints of the arcs lensed by MACS J1149+2223 are identical to those in J14 (Figure 1), except for the main lensed source in this cluster,

kerens@umich.edu

\*Based on observations made with the NASA/ESA *Hubble Space Telescope*, obtained from the Data Archive at the Space Telescope Science Institute, which is operated by the Association of Universities for Research in Astronomy, Inc., under NASA contract NAS 5-26555. These observations are associated with programs GO-9722, GO-12065

<sup>1</sup>Department of Astronomy, University of Michigan, 1085 S. University Ave., Ann Arbor, MI 48109, USA

<sup>3</sup> <http://archive.stsci.edu/prepds/frontier/lensmodels/>

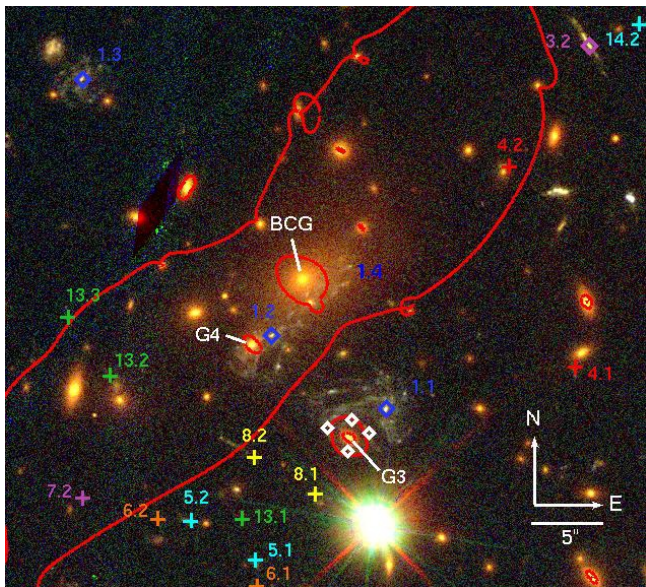


FIG. 1.— Color composite image of the core of strong lensing cluster MACS J1149+2223 from *HST*/ACS F814W (red), F606W (green), F435W (blue). The critical curves of the best-fit lens model are plotted in red for  $z = 1.491$ . The multiply imaged lensed sources that are used as constraints are color coded and labeled, with diamonds for sources with spectroscopic redshifts, and crosses for sources for which only photometric redshifts are available. For a full list of these images, including their coordinates, see J14. The three full images and fourth partial image of the host galaxy are labeled in blue, and the positions of the multiply-imaged lensed SN are marked with white diamonds next to image 1.1. The constraints within the images of source 1 are shown in Figure 2

the face-on spiral galaxy at  $z = 1.491$  that hosts “SN Refsdal”. The constraints that we used in J14 did not favor this galaxy over other lensed sources, and used as lensing evidence only the brightest emission knot in each of the three full images of the source (1.1, 1.2 and 1.3 in Figures 1 and 2). Here, we take full advantage of morphological information and use as constraints several emission knots on the spiral arms of each of the lensed images of this galaxy. Figure 2 shows the lensing constraints that are used in this model.

The identification and mapping of the knots between the lensed images of this galaxy are aided by the lens model of J14, and constructed iteratively as higher levels of the current model were computed. Our identifications are done independently from those in Smith et al. (2009) and Rau et al. (2014), but are in general agreement with their identifications. With our final model, many more features can be identified (e.g., Rau et al. 2014); the features that are used as constraints here provide a uniform spatial coverage of the galaxy.

To the morphological constraints we add the positions of the four images of the SN from Kelly et al. (2014a), which appear around the cluster galaxy G3.

We note that the bright emission knot next to G4 is not used as a constraint in this model; the source reconstruction (see Section 3) supports the association of this knot, as well as other clumps East of G4, with secondary lensing by G4 that complicates image 1.2, as suggested by Zitrin et al. (2009) and Rau et al. (2014). However, since this knot is in close proximity to the critical curve of G4 we cannot determine whether it is indeed a counter image of the core of the lensed galaxy, or a

different region that falls on the caustic and is therefore highly magnified. In total, there are three full images of the host galaxy, and additional images of some of the emission knots that form a partial fourth image West of the brightest cluster galaxy (BCG), and a partial image near G4.

The mass distribution is composed of the five pseudo-isothermal elliptical mass distribution (PIEMD) halos in J14, with two additional halos that were individually optimized as described below. With the increased number of constraints around the images of source 1, we increase the flexibility of the model in these areas by freeing the parameters of the cluster galaxies closest in projection to 1.1 and 1.2. In particular, we allow the model to fit for the ellipticity, position angle, core and cut radii, and velocity dispersion of the galaxy that lenses the SN (G3), as well as the core, cut radii and velocity dispersion of the two central galaxies at the core of the cluster (BCG, G4). We also free some parameters that were fixed in J14 to be fitted by the model; however, we find that these parameters are consistent with the fixed values of J14.

Cluster galaxies are also included in the mass model as PIEMD halos, with parameters scaled with their luminosity. J14 used the cluster galaxies from Smith et al. (2009), selected from *K*-band imaging data. In order to increase the accuracy of the astrometric positioning of the cluster galaxies, we construct our galaxy catalog directly from the archival *HST* imaging, taken as part of the CLASH multicycle program (PI: Postman; Postman et al. 2012) and GO-9722 (PI: Ebeling; Smith et al. 2009). Cluster galaxies are selected from the *HST* ACS/F606W and F814W photometry as those with  $F606W - F814W$  colors that place them on the cluster red sequence in a color-magnitude diagram. We assume  $m_* = 20.04$  in ACS/F814W. The coordinates, ellipticity, and position angle of the cluster galaxies are fixed to their observed values, and the other parameters are scaled with their luminosity (see Limousin et al. 2005 for a description of the scaling relations). Our final model includes 116 constraints and 38 free parameters (Table 1). Among the constraints are three spectroscopic redshifts of lensed galaxies. The redshifts of the other nine lensed galaxies are set as free parameters, with priors based on their photometric redshifts from Jovel et al. (2013).

### 3. RESULTS AND CONCLUSIONS

Figure 1 shows the critical curves of the best fit model over-plotted on a color image of the core of MACS J1149+2223. We find a significantly smaller scatter in the image plane for the lensed galaxy that hosts “SN Refsdal”, with a typical scatter of  $0''.15$  for individual emission knots. The image plane scatter of image 1.1 is reduced from  $0''.83$  in J14 to  $0''.03$  here. The lens model products are available to the community through the HFF modeling page on MAST.

We reconstruct the source-plane image of the host galaxy using methods described in Sharon et al. (2012, 2014), by ray-tracing the pixels of each image of the lensed galaxy to the source plane. As can be seen in Figure 3, the three source reconstructions are in excellent agreement. We ray-trace the position of the SN through the best-fit lens model from the observed positions near

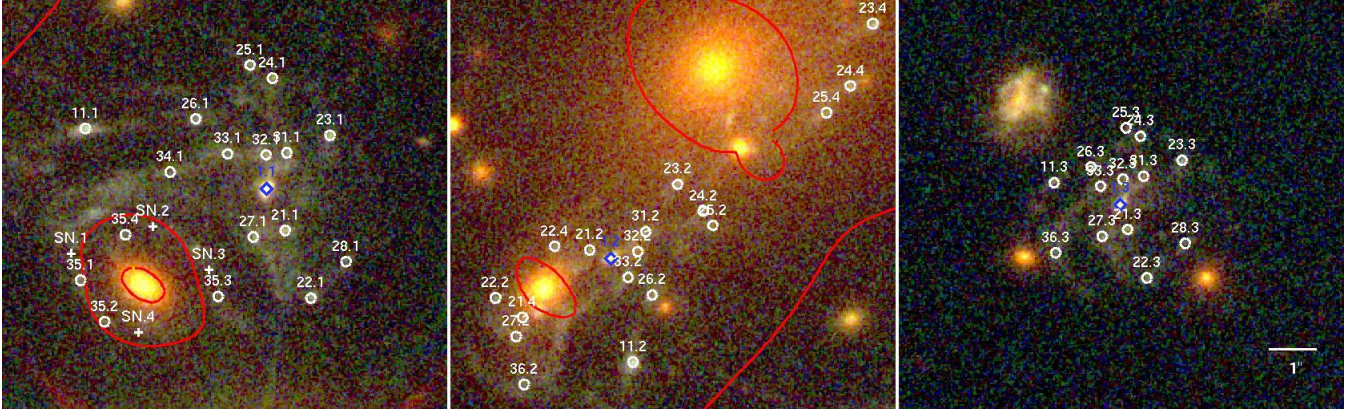


FIG. 2.— Zoom in view on the three full images of the host galaxy; the emission knots that were used as constraints in this model are marked, as well as the SN positions from Kelly et al. (2014a).

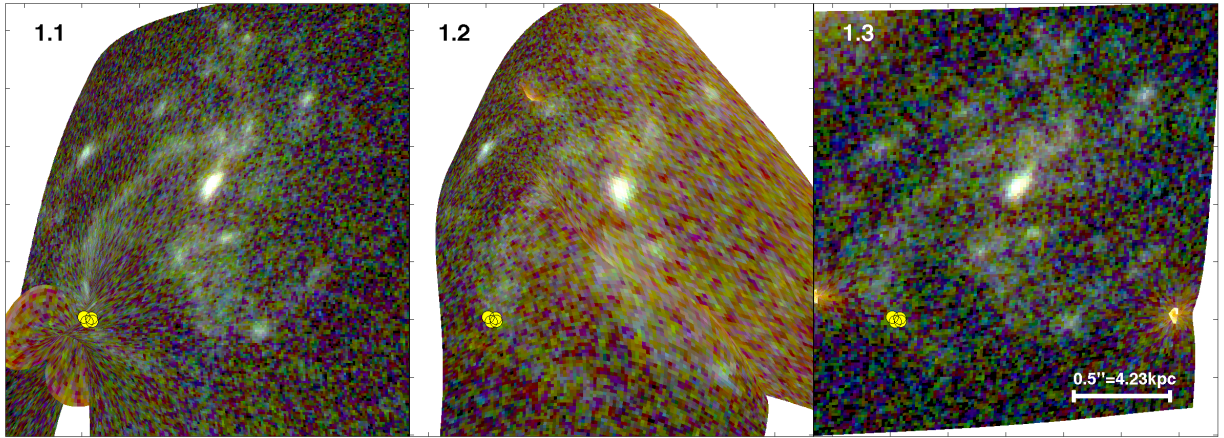


FIG. 3.— Source reconstructions from the three full images of the host galaxy are in excellent agreement. The positions of the SN images are ray-traced from image 1.1 to the source plane, and marked in yellow circles on all the source images, indicating that it most likely occurred in one of the spiral arms. Ghost-like features appear as a result of ray-tracing of light from the foreground galaxies.

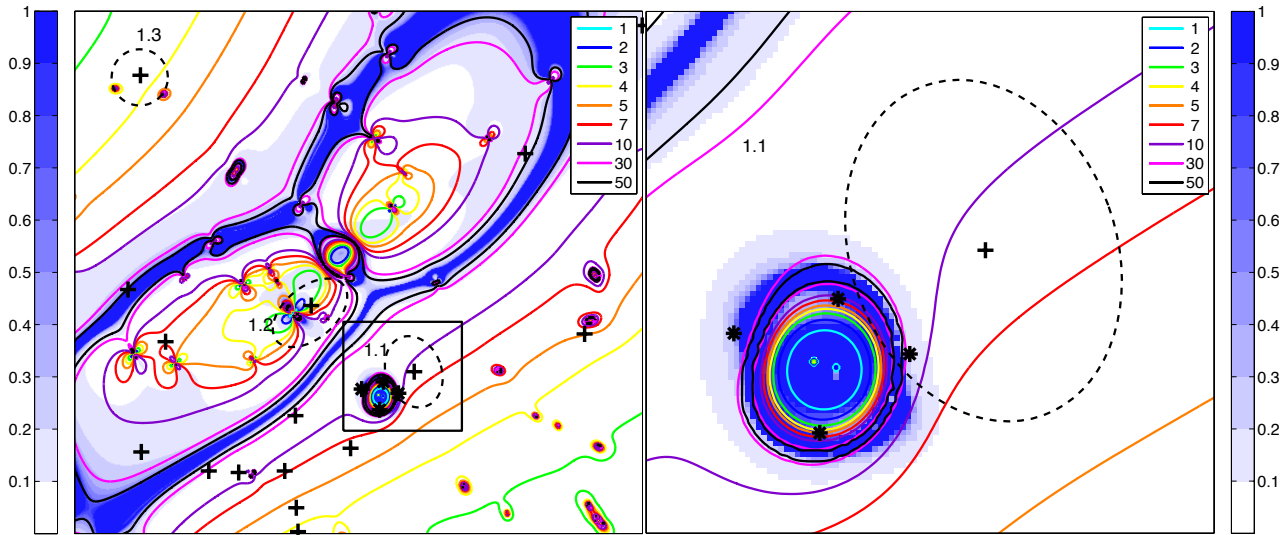


FIG. 4.— The magnification and its uncertainty for a source at  $z=1.491$ . The contours indicate the value of the magnification, and the color gradient indicates the uncertainty in the magnification in each position. The uncertainty is given in units of  $\Delta\mu/\mu$ . The field of view and scale are the same as those in Figure 1 and Figure 2 for the left and right panels respectively. To guide the eye, we plot the positions of the images of the lensed sources with black crosses, and the SN positions in black asterisks.

G3, to the other images of the lensed galaxy. We find that the SN most likely occurred in one of the spiral arms of this galaxy (Figure 3). The source reconstruction is in good agreement with the results of Rau et al. (2014), who used a surface brightness distribution modeling approach.

Figure 4 maps the magnification ( $\mu$ ) and its fractional uncertainty ( $\Delta\mu/\mu$ ) for a source at  $z = 1.491$ . We find a magnification of  $9.61_{-0.95}^{+1.00}$  at the location of the brightest emission knot of image 1.1; at the location of the four images of the SN, the magnifications are somewhat higher, due to the added lensing boost from G3,  $\mu(S1) = 18.99_{-4.97}^{+5.96}$ ,  $\mu(S2) = 12.94_{-4.09}^{+8.93}$ ,  $\mu(S3) = 22.46_{-5.82}^{+17.14}$ ,  $\mu(S4) = 10.30_{-3.49}^{+7.57}$ , for images S1, S2, S3, S4, respectively. We note that microlensing by the galaxy G3 may contribute to the magnification of some of the lensed images of the SN (Schechter & Wambsganss 2002).

The time delay predictions are given with respect to image a of the SN:  $\Delta t_{S2-S1} = -42_{-12}^{+65}$ ,  $\Delta t_{S3-S1} = 33_{-48}^{+124}$ ,  $\Delta t_{S4-S1} = 45_{-119}^{+131}$  days. The time delay between S1 and the predicted location of the SN in the other lensed images of the host galaxy are of order years, with  $\Delta t_{1.2-S1} = 1326_{-220}^{+223}$  days and  $\Delta t_{1.3-S1} = -4878_{-398}^{+337}$  days. We note that the model does not use time delays as constraints; at the time of this publication, time delays have not yet been measured. The relatively short time delays that are predicted by the lens model are consistent with the detection of three images of this SN at the same time. In the SN restframe, these time delays are shorter by a factor of  $(1+z)$ , and amount to about 2 weeks.

In addition to lensing by the cluster potential, a small part of the spiral arm in which the SN appears is lensed by the nearby cluster galaxy, G3, forming a ring around it. The archival data are not deep enough to uniquely identify substructure in this ring, but it will likely be feasible with the full depth of the Hubble Frontier Field imaging. Nevertheless, the accurate positions of the newly discovered SN on this ring can be used as constraints to model the mass distribution in this cluster galaxy. We find that the galaxy is well described by a PIEMD halo centered on the observed light distribution (Table 1).

We expect that the full depth of the HFF observation of MACS J1149+2223 will reveal ample new lensing constraints as new background sources are detected. These constraints will be most useful for reducing the uncertainties in the mass model of the cluster (e.g., Jauzac et al. 2014a, 2014b).

The discovery of a multiply imaged variable source with resolved images has interesting implications on constraining the mass distribution of its foreground lens. Follow up photometric observations of this source will reveal the time delay between the images, and measure their relative magnifications. Adding these unique SN constraints to the positional constraints can improve the lens model of G3 and the cluster in which it is embedded (e.g., Nordin et al. 2014). Such future analysis has the potential to constrain the truncation radius of the galaxy due to tidal stripping, measure the slope of its mass distribution, and the correlation between stellar mass and dark matter distributions, all of which can inform studies of galaxy evolution in cluster environment.

## REFERENCES

- Ebeling, H., Barrett, E., Donovan, D., et al. 2007, *ApJ*, 661, L33  
 Goobar, A., Paech, K., Stanishev, V., et al. 2009, *A&A*, 507, 71  
 Kovner, I., & Paczynski, B. 1988, *ApJ*, 335, L9  
 Jauzac, M., Clément, B., Limousin, M., et al. 2014a, *MNRAS*, 443, 1549  
 Jauzac, M., Richard, J., Jullo, E., et al. 2014b, arXiv:1409.8663  
 Johnson, T. L., Sharon, K., Bayliss, M. B., et al. 2014, (J14), *ApJ*, 797, 48  
 Jouvel, S., Host, O., Lahav, O., et al. 2013, *VizieR Online Data Catalog*, 356, 29086  
 Jullo, E., Kneib, J.-P., Limousin, M., Elíasdóttir, Á., Marshall, P. J., & Verdugo, T. 2007, *New Journal of Physics*, 9, 447  
 Kelly, P., Rodney, S., Treu T., et al. 2014, *The Astronomer's Telegram*, 6729, 1  
 Kelly, P., Rodney, S., Treu T., et al. 2014, arXiv:1405.6009  
 Kovner, I., & Paczynski, B. 1988, *ApJ*, 335, L9  
 Limousin, M., Kneib, J.-P., & Natarajan, P. 2005, *MNRAS*, 356, 309  
 Nordin, J., Rubin, D., Richard, J., et al. 2014, *MNRAS*, 440, 2742  
 Patel, B., McCully, C., Jha, S. W., et al. 2014, *ApJ*, 786, 9  
 Quimby, R. M., Oguri, M., More, A., et al. 2014, *Science*, 344, 396  
 Rau, S., Vegetti, S., & White, S. D. M. 2014, *MNRAS*, 443, 957  
 Refsdal, S. 1964, *MNRAS*, 128, 307  
 Richard, J., Jauzac, M., Limousin, M., et al. 2014, *MNRAS*, 444, 268  
 Schechter, P. L., & Wambsganss, J. 2002, *ApJ*, 580, 685  
 Sharon, K., Gladders, M. D., Rigby, J. R., et al. 2012, *ApJ*, 746, 161  
 Sharon, K., Gladders, M. D., Rigby, J. R., et al. 2014, *ApJ*, 795, 50  
 Smith, G. P., Ebeling, H., Limousin, M., et al. 2009, *ApJ*, 707, L163  
 Zitrin, A., & Broadhurst, T. 2009, *ApJ*, 703, L132  
 Zitrin, A., Broadhurst, T., Barkana, R., Rephaeli, Y., & Benítez, N. 2011, *MNRAS*, 410, 1939  
 Zitrin, A., Fabris, A., Merten, J., et al. 2014, arXiv:1411.1414

TABLE 1  
BEST-FIT LENS MODEL PARAMETERS

Component	$\Delta$ RA ( $''$ )	$\Delta$ Dec ( $''$ )	$e$	$\theta$ (deg)	$r_{\text{core}}$ (kpc)	$r_{\text{cut}}$ (kpc)	$\sigma_0$ (km s $^{-1}$ )
cluster halo 1 (H1)	$10.5^{+1.1}_{-1.4}$	$-6.85^{+1.21}_{-0.83}$	$0.61^{+0.01}_{-0.10}$	$23.8^{+4.8}_{-2.3}$	$125^{+7}_{-15}$	[1500]	$914^{+69}_{-60}$
cluster halo 2 (H2)	$-13.2^{+1.6}_{-1.4}$	$27.3^{+0.9}_{-4.4}$	$0.30^{+0.05}_{-0.14}$	$67.5^{+21.6}_{-5.5}$	[50]	[1500]	$923^{+48}_{-79}$
BCG (BCG)	[0]	[0]	$0.69^{+0.07}_{-0.10}$	$33.6^{+6.0}_{-0.1}$	$9.59^{+0.41}_{-2.19}$	[200]	$416^{+17}_{-28}$
cluster galaxy 1 (G1)	[25.6]	[-32.2]	[0.205]	[47.0]	[0.233]	[40.2]	$527^{+31}_{-37}$
cluster galaxy 2 (G2)	$17.0^{+0.0}_{-0.5}$	$101 \pm 1$	[0.8]	$-54.4^{+1.0}_{-14.1}$	[0.261]	[300]	$355^{+60}_{-2}$
cluster galaxy 3 (G3)	[3.162]	[11.088]	$0.36^{+0.40}_{-0.17}$	$-34.2^{+2.9}_{-5.8}$	$0.16^{+2.93}_{-0.16}$	$3.60^{+1.09}_{-1.58}$	$235^{+87}_{-11}$
cluster galaxy 4 (G4)	[3.648]	[-4.568]	[0.355]	[48.3]	$1.34^{+1.29}_{-1.31}$	$3.67^{+7.36}_{-1.92}$	$209 \pm 67$
L* galaxy	...	...	...	...	[0.15]	[30]	[150]

NOTE. — All the coordinates are measured in arcseconds East and North of the center of the BCG, at [RA, Dec]=[177.39875 22.398531]. Mass components are all PIEMD. The ellipticity of the projected mass density is expressed as  $e = (a^2 - b^2)/(a^2 + b^2)$ .  $\theta$  is measured North of West. Error bars correspond to 1- $\sigma$  confidence level as inferred from the MCMC optimization. Values in square brackets are for fixed parameters that were not optimized. The location and the ellipticity of the matter clumps associated with the cluster galaxies were kept fixed according to their light distribution, and the other parameters determined through scaling relations (see text). Halo and galaxy notations are adopted from J14. G3 is the cluster galaxy closest to image 1.1, and G4 is the cluster galaxy closest to image 1.2.